Int. J. Electrochem. Sci., 16 **(2021)** Article ID: 210464, doi: 10.20964/2021.04.64

International Journal of
ELECTROCHEMICAL
SCIENCE
www.electrochemsci.org

Effective Electrochemical Sensor Based on Au Nanoparticles Decorated Carboxylated Multi-wall Carbon Nanotube (AuNPS@c-MWCNTs) Nanocomposites for Determination of Dicapthon Pesticide in Agricultural Food

Lei Wang, Yao Liu, Yufei Chen[*]

School of Cereal, Jilin Business and Technology College, Changchun 130507, China
[*]E-mail: chenyufei202012@sina.com

Received: 2 January 2021 / *Accepted:* 24 February 2021 / *Published:* 28 February 2021

This study was focused on the preparation and characterization of nanocomposite Au nanoparticles and carboxylated MWCNTs (Au NPs@c-MWCNTs) as electrochemical sensors for determination of dicapthon pesticide in agricultural food samples. Au NPs@c-MWCNTs nanocomposite was electrodeposited on glassy carbon electrode (GCE). The morphology and crystal structure of the modified electrode were characterized by SEM and XRD analyses, which indicated that the spherical Au NPs in fcc crystal structure were uniformly distributed on inter-connected network-like structure of c-MWCNTs. The electrochemical characterization of bare GCE, MWCNTs/GCE and Au NPs@c-MWCNTs/GCE by cyclic voltammetry (CV) and differential pulse voltammetry (DPV) techniques showed that the Au NPs@c-MWCNTs/GCE had more stable, sharp signal toward dicapthon. Au NPs@c-MWCNTs/GCE exhibited excellent selectivity, high stability, the acceptable detection limit (0.09 μg/l) and linear range (0 to 2400 μg/l) for determination of dicapthon. The capability of Au NPs@c-MWCNTs/GCE was evaluated for dicapthon detection in cabbage as a real sample. The results showed an improvement in electrochemical sensing properties of Au NPs@c-MWCNTs/GCE which can be attributed to the electron-transfer enhancement between analyte and electrode surface due to interface efficiently of MWCNTs and Au NPs and large surface area of Au NPs and their highly conductive nature.

Keywords: Nanocomposite; Au nanoparticles; Carboxylated MWCNTs; Electrochemical sensor; Dicapthon; Agricultural food

1. INTRODUCTION

Organophosphorus pesticides as strong nerve poisons can degrade microorganism through inhibiting acetylcholinesterase enzymes, which not only are commonly vital for normal insect's physiology, but also hydrolyzes choline esters in human body and important in the brain's development

[1, 2]. These pesticides have been developed to substitute the organ halide pesticides due to relatively higher biodegradation rate processes[3].

The killing organophosphates agents have been used for synthesis of more than 50% of chemical pesticides which lead to public concern for management of the application of pesticides in agriculture, forestry, urban, and public health spraying[4, 5]. Phosmet, dichlorvos, diazinon, chlorpyrifos, fenthion, Malathion, parathion, methyl parathion, tetrachlorvinphos, aldicarb, carbofuran, azamethiphos, and azinphos-methyl are the most applicant organophosphorus pesticides[6]. Dicapthon (Phosphorothioic acid 0-(2-chloro-4-nitrophenyl) 0.0-dimethyl ester) as an expensive cholinesterase inhibitor is also classified in organophosphorus pesticides[7]. The chloro-4-nitrophenyl in dicapthon isahighly toxic compound that can inhibit P-glycoprotein activity in humans and animals which acts as a localized drug transport mechanism, actively exporting drugs out of the cell [8, 9].

Besides, release of organophosphorus pesticides into the environment can cause risk of poisoning, impaired memory, impaired memory, irritability, confusion, headache, mutagenicity, premature fetus, cognitive and behavioral deficits in children, carcinogenicity, lung issues and immunotoxicity[10, 11]. Thus, the environmental protection agency considered organophosphorus as the first class of pesticides and placed new restrictions on the use of the organophosphates to protect agricultural workers.

Furthermore, many studies have been done on determination of organophosphorus pesticides in vegetables, fruits, food products, municipal and industrial wastewater by thin-layer chromatography, gas chromatography–flame photometry, high-performance liquid gas chromatography, capillary gas chromatography–mass spectrometry, immunochemical and electrochemical techniques [12]. Simpleness, inexpensiveness and speed of electrochemical methods make them the favorite techniques for kinetics of electron transfer and characterization redox activity as electrochemical response for determination of pesticides [13-19]. Moreover, modification of sensor electrodes with nanostructured materials not only can miniaturize the sensor system, but also improves the sensor performance in gaseous or aquatic environments [16, 20]. The great surface area and porosity of nanostructured films provides more active site and excellent electron transfer efficiency [21-24]. Therefore, this study was conducted on preparation and characterization of effective electrochemical sensors based on Au NPs@c-MWCNTs for determination of dicapthon pesticide in agricultural food.

2. EXPERIMENT

Prior the modification of GCE (Wuhan Corrtest Instruments Corp., Ltd., China), it was polished with 0.3 µm alumina slurry (96%, Yangzhou ZTL New Materials Co., Ltd., China) for 15 minutes, washed ultrasonically by deionized water (15 minutes) and ethanol (10 minutes), respectively, and dried in room temperature. The cleaned GCE was electrodeposited in prepared mixture of 1 g/l MWCNTs (96%, outer diameter 20-40 nm and length 10-30 µm, Xingtai Shineway Corporation Co., Ltd., China) and 0.2 M H_2SO_4 (96%, Qingdao Hisea Chem Co., Ltd., China) solution containing 0.1 M phosphate buffer solution (PBS) and $AuCl_4.3H_2O$ (≥99.9% trace metals basis, Sigma-Aldrich) with 0, 2 mM, 5 mM and 8mM concentrations referred to S0, S1, S2 and S3, respectively, under applied potential from -0.8 V to 0.8 V at scan rate of 15 mV/s for 20 minutes at room temperature. The MWCNTs were carboxylated in H_2SO_4 solution and concurrently nanocomposite of Au NPs@c-MWCNTs was directly electrodeposited on the GCE surface.

Morphology and structural characterizations of prepared electrodes were considered by scanning electron microscopy (SEM, JSM-6701F, JEOL, Japan) and X-ray diffraction (XRD, Philips X'Pert Pro MPD, CuKα (λ=1.5418 Å)), respectively. CV and DPV electrochemical measurements were conducted on electrochemical working station (Autolab PGSTAT204) in conventional three-compartment electrochemical cell was employed Ag/AgCl as the reference electrode, Pt as a counter electrode, and prepared electrode (bare GCE, MWCNTs/GCE and Au NPs@c-MWCNTs/GCE) as working electrode. Electrochemical studies was conducted in 0.1 M phosphate buffer solutions (PBS) and 0.1M PBS containing $[Fe(CN)_6]^{3-/4-}$ (99%, Haihang Industry Co., Ltd., China). 0.1M PBS prepared of 0.1 M H3PO4 (≥85%, Lerona Imp. & Exp. Ltd., China) and 0.1 M NaH_2PO_4 (99%, Sigma-Aldrich).

Fresh cabbage was purchased from a local supermarket, washed with water, and sliced. 40 µg/l dicapthon solutions were sprayed onto slices of cabbage. All of the slices were transferred to juicer and cabbage juice was extracted. Then, the extracted juice was centrifuged for 10 minutes at 2000 rpm. 1l of obtained liquid phase was mixed with1l of 0.1 M PBS solution. The prepared real sample was stored in the refrigerator at 5°C for subsequent measurements.

3. RESULTS AND DISCUSSION

SEM images in Figure 1 reveal the surface morphologies of the modified c-MWCNTs and Au NPs@c-MWCNTs nanocomposite electrodes. The morphology of MWCNTs film shows an interconnected network-like structure of c-MWCNTs with diameter range from 40 to 60 nm and length range from 15-30 µm. The morphologies of Au NPs@c-MWCNTs films exhibit that spherical Au NPs as bright spots are uniformly distributed in entangled texture of MWCNTs. Thus, SEM images evidence of strong interactions between Au NPs on MWCNTs.

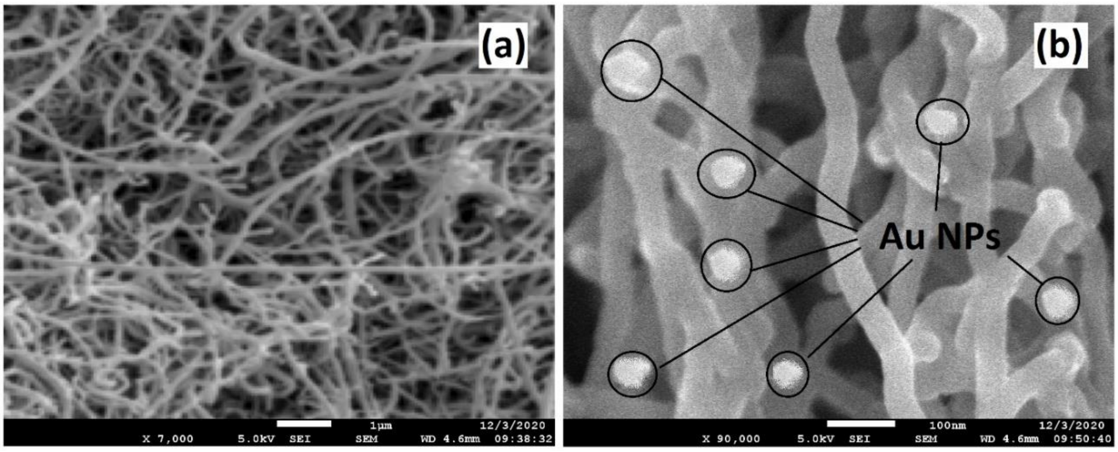

Figure 1. SEM images of (a) MWCNTs and (b) Au NPs@c-MWCNTs modified GCE

The obtained XRD patterns of c-MWCNTs and Au NPs@c-MWCNTs nanocomposite powders are presented in Figures 2. For Au NPs@c-MWCNTs nanocomposite (S1 to S3), XRD patterns shows diffraction peak at 38.38, 44.57, 64.88 and 78.79° can be assigned to the (111), (200), (220) and (311) crystalline planes, respectively, which corresponded to fcc crystal structured Au NPs (JCPDS card No 04-0784). As seen, the strong diffraction peak at 26.19° in all samples is associated with the graphitic signature of c-MWCNTs with (002) crystalline plane (JCPDS card No.75-1621) which demonstrated strong bonded Au NPs on c-MWCNTs walls in agreement with the SEM results.

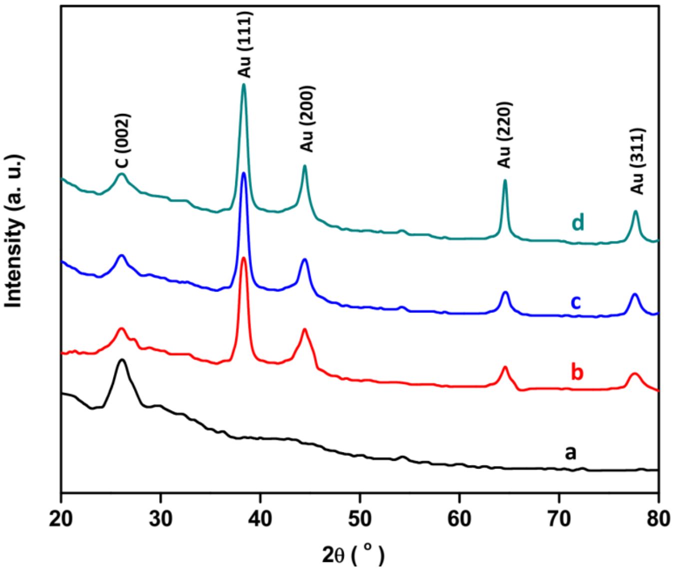

Figure 2. XRD patterns Au NPs@c-MWCNTs powders (a) S0, (b) S1, (c) S2, and (d) S3.

The electrochemical CVs response of bare GCE, c-MWCNTs and Au NPs@c-MWCNTs nanocomposite modified GCE are shown in Figure 3 under applied potential from -0.4V to 0.4V at scan rate of 50mV/s in 0.1M PBS (pH7.0) including 5mM $[Fe(CN)_6]^{3-/4-}$ as the redox probe. As seen, the anodic peak currents are obtained of 0.37, 0.61, 1.20, 1.72 and 1.96 µA at 0.11, 0.11, 0.08, 0.10 and 0.03 V for bare GCE, S0, S1, S2 and S3, respectively. Moreover, the cathodic peak currents are recorded of -0.51, -1.03, -1.43, -2.13 and -1.94 µA at -0.01, -0.01 , 0.01 , 0.00 and 0.02 V for bare GCE, S0, S1, S2 and S3, respectively. The higher currents of redox peaks are observed for S2 and S3 samples because of the deeply entrapped Au NPs into the c-MWCNTs structure and improvement of conductivity of the prepared electrodes and effective surface area [25, 26]. In addition, with increasing the Au concentration in nanocomposite, the anodic peak potential is shifted toward lower potential because of facilitation in electron transfer [25, 26]. The lower anodic and cathodic potentials belong to the S2 sample.

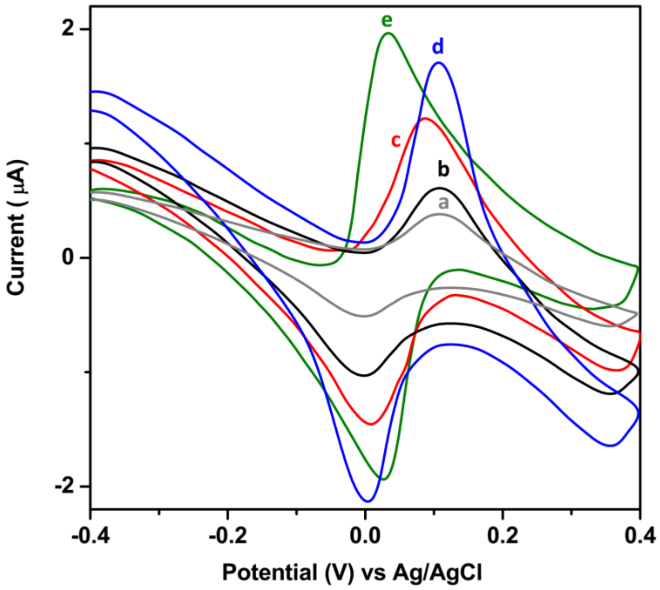

Figure 3. The electrochemical CVs response of (a) bare GCE, (b) S0, (c) S1, (d) S2, and (e) S3 at scan rate of 50mV/s in 0.1M PBS (pH7.0) including 5mM $[Fe(CN)_6]^{3-/4-}$.

Figure 4 shows the recorded CVs and plots of redox peak currents vs. square root of scan rate prepared electrodes at scan rates of 10, 20, 50, 80 and 50mV/s in 0.1M PBS (pH7.0) including 5mM $[Fe(CN)_6]^{3-/4-}$. Considerable enhancement peak current was recorded with increasing the scan rate values. The plots of peak currents versus square root of scan rates demonstrates a linear relationship which reveals the reaction between the surface of electrode and electrolyte is quasi-reversible and diffusion process controlled [27]. The effective surface area for electrodes can be calculated by the Randles-Sevcik formula [28, 29]:

$$I_p = 2.69 \times 10^5\, n^{3/2}\, A\, D^{1/2}\, C\, \nu^{1/2} \qquad (1)$$

Where I_p (A) is peak current density, n is the number of electrons that transferred in the redox process (n=1), A (cm^2) is the electroactive surface area, D (6.5×10^{-6} cm^2/s) is the diffusion coefficient of $[Fe(CN)_6]^{3-/4-}$, C(mol/cm^3) is electroactive catalytic species, ν (V/s) is scan rate. Therefore, effective surface areas of S0, S1, S2 and S3 can be calculated 1.54×10^{-3}, 1.70×10^{-3}, 1.15×10^{-3}, and $4.27 \times 10^{-4} cm^2$, respectively from slopes of anodic peak current vs. $\nu^{1/2}$. Accordingly, the S2 sample shows the higher effective surface area. Thus, further electrochemical measurements were performed on S2 samples as Au NPs@c-MWCNTs/GCE.

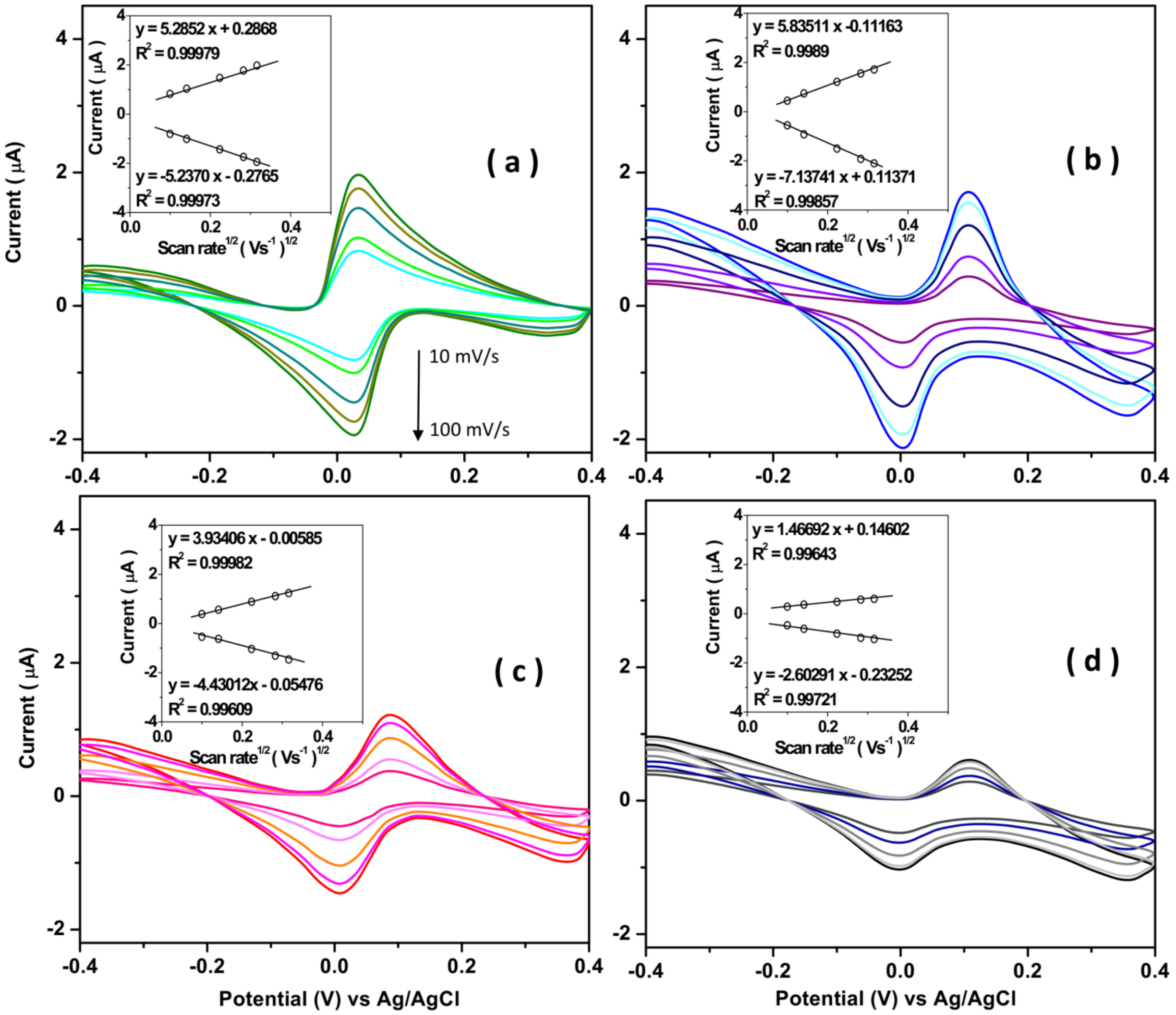

Figure 4. The recorded CVs and plots of redox peak currents vs. square root of scan rate of (a) S0, (b) S1, (c) S2, and (d) S3 at scan rates of 10, 20, 50, 80 and 50mV/s in 0.1M PBS (pH7.0) containing 5mM $[Fe(CN)_6]^{3-/4-}$.

The first, second and third recorded CVs of Au NPs@c-MWCNTs/GCE under applied potential from -0.8 to 0.7V at scan rate of 10 mV/s in 0.1M PBS (pH7.0) including 1200µg/l dicapthon are shown in Figure 5. As observed from the first cycle, there is an obvious irreversible reduction peak at -0.35 V (peak I), which attributed to the reduction of the nitro group to hydroxylamine group with $4e^-$ [30, 31] which Subsequently oxidized to the nitroso group at potential of 0.14 V (peak II). Another reduction peak at 0.20 V (peak III) appears in the second recorded CV that is assigned to reverse reaction of process in peak II. The reversible redox peaks (II and III) are allocated to a two-electron-transfer process [30, 31]. As seen from the second and third recorded CVs, the reduction peak I disappeared which ascribed to the reaction exhaustion of dicapthon on Au NPs@c-MWCNTs/GCE surface. These electrochemical reactions are in agreement with the reported electrochemical mechanism of nitroaromatic compounds [30-32].

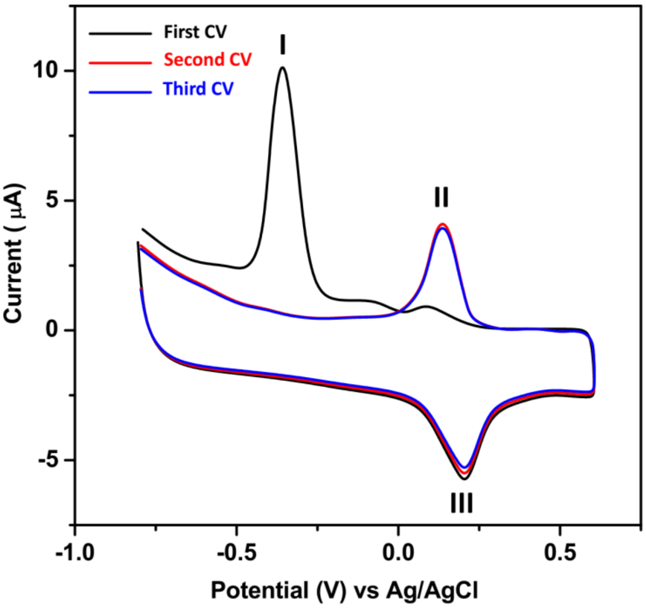

Figure 5. The first, second and third recorded CVs of Au NPs@c-MWCNTs/GCE in 0.1M PBS (pH7.0) including 1200µg/l dicapthon.

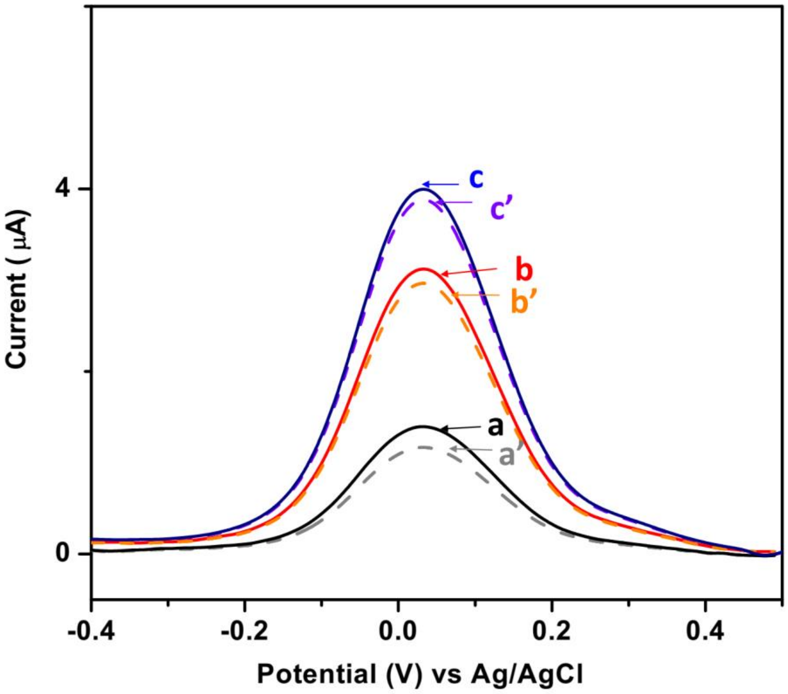

Figure 6. The first and 50th recorded DPVs for determination of dicapthon on the (a, a') bare GCE, (b, b') MWCNTs/GCE and (c, c') Au NPs@c-MWCNTs/GCE in 0.1M PBS (pH7.0) including 1200µg/l dicapthon

According to an accepted mechanism for the electrochemical reduction of nitroaromatic compounds, voltammetric peak is attributed to $4e^-$ reduction process of dicapthon [31]. This electrochemical reduction may be caused by the adsorption of dicapthon or its reductive product on electrode surfaces, and may inactivate the electroactive sites on electrode surfaces [31]. Therefore, the stability of prepared electrodes was examined through successive scans of electrochemical responses of electrodes to presence of dicapthon. DPVs measurements was recorded for determination of dicapthon on the bare GCE, MWCNTs/GCE and Au NPs@c-MWCNTs/GCE under applied potential from -0.4 to 0.5V at scan rate of 10mV/s in 0.1M PBS (pH7.0) including 1200μg/l dicapthon. In Figure 6, there are reduction peaks at 0.03 V for first recorded DPVs of all electrodes (6a, 6b and 6c). The 50th recorded DPVs reveal the decrease of peak current of 15%, 6% and 3% for bare GCE (6a'), MWCNTs/GCE (6b') and Au NPs@c-MWCNTs/GCE (6c'), respectively. In addition, the DPV of Au NPs@c-MWCNTs/GCE displays more stable, sharp and higher reduction peak current which is related to enhancement of electron transfer between analyte and electrode surface due to interface efficiently of MWCNTs and Au NPs [33]. It can be related to the large surface area of Au NPs and their highly conductive nature [34]. Moreover, MWCNTs can serve as a robust support for the stabilization of Au NPs [35].

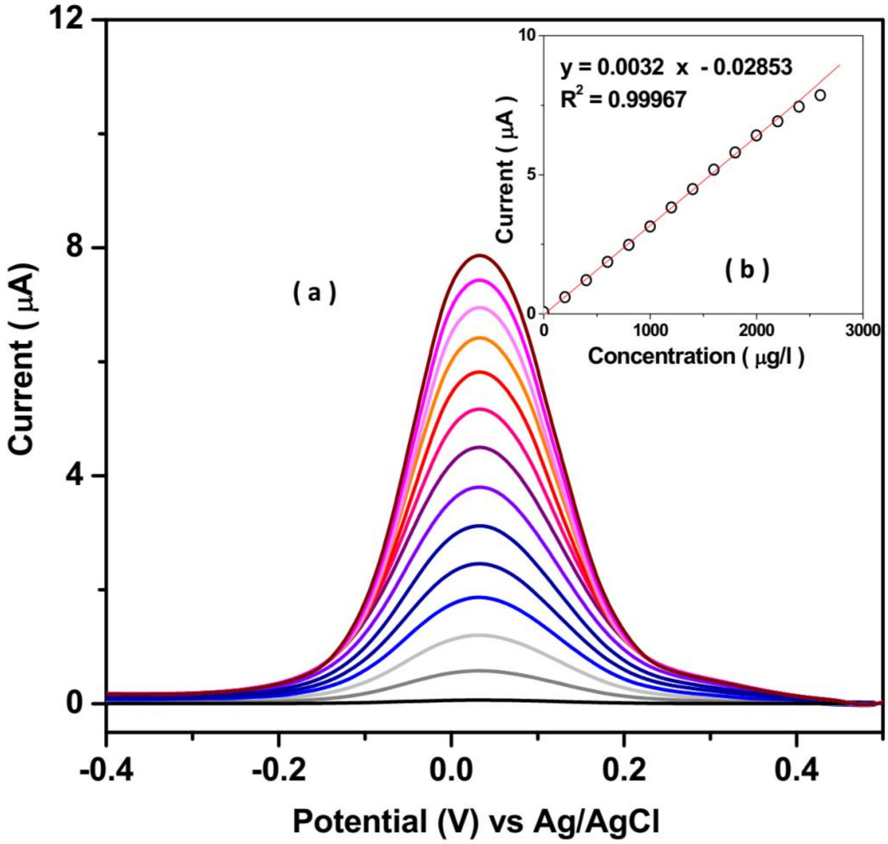

Figure 7. (a) The recorded DPVs and (b) calibration plot of Au NPs@c-MWCNTs/GCE to addition of dicapthon concentration in 0.1M PBS (pH7.0).

As shown in Figure 7a, for Au NPs@c-MWCNTs/GCE, the increase the dicapthon concentration causes to the increase the reduction peak current at 0.03 V The calibration plot in Figure 7b shows the linear relationship between the dicapthon concentration and linear electrocatalytic current at ranging from 0 to 2400 µg/l. Furthermore, detection limit is obtained 0.09 µg/l. The obtained detection limit and linear range for determination of dicapthon on Au NPs@c-MWCNTs/GCE are compared with other reported organophosphate pesticides sensing systems in Table 1 that it shows the analytical performance of the Au NPs@c-MWCNTs/GCE is competitive to the reported organophosphate pesticides sensing systems. Moreover, the high stability and high conductivity of Au NPs and c-MWCNTs can provide the sensitive sensor for dicapthon. Limited studies have been conducted in for determination of dicapthon by electrochemical technique (SWCNTs/Nafion/GCE with detection limit of 36 µg/l) [31], accordingly, use of Au NPs@c-MWCNTs/GCE a electrochemical sensor with very low detection limit (0.09 µg/l) can be novelty for the detection of dicapthon.

Table 1. Comparison between the obtained detection limit and linear range of dicapthon on Au NPs@c-MWCNTs/GCE and the reported organophosphate pesticides sensing systems

Electrode	**organophosphate pesticide**	**Technique**	**Linear Range (µg/l)**	**Limit of detection (µg/l)**	**Ref.**
MWCNT/Nafion/GCE	parathion	Amp[a]	1.456 to 5826	1.747	[36]
functionalized graphene quantum dot	parathion	EIS[b]	0.00001 to 0.106	4.6×10^{-5}	[37]
Cd nano-metal organic framework /ITO	parathion	EIS	0.1 to 20	0.1	[38]
conducting poly([2,2″;5″ 2″]-terthiophene-3′-carbaldehyde)/GCE	malathion	CV	4950 to 543100	1.18	[39]
CuO nanowires/CNT	malathion	EIS	0 to 39.64	0.099	[40]
CdTe quantum dots/cetyltrimethylammonium bromide	methyl parathion	FP[c]	25 to 3000	18	[41]
MoS_2/grapheme/GCE	methyl parathion	Amp	2632 to 500000	8.42	[42]
CNT/GCE	Methyl parathion	DPV	5.264 to 26.321	0.263	[43]
reduced graphene oxide/GCE	Methyl parathion	SWV[d]	0.789 to 5.26	0.233	[14]
reduced graphene oxide /Nafion/GCE	Methyl parathion	SWV	0.526 to 184.247	0.263	[13]
Acetylcholinesterase/Au nanoshpere	Methyl Parathion	CV	6.580 to 78.963	0.315	[15]
Carbon Black nanoparticles	paraoxon	CV	5 to 30	5	[44]
SWCNTs/Nafion/GCE	dicapthon	DPV	200 to 60000	36	[31]
Au NPs@c-MWCNTs/GCE	dicapthon	DPV	0 to 2400	0.09	This work

[a]Amp: Amperometry[b]EIS: Electrochemical impedance spectroscopy

[c]FP: Fluorescence probing [d]SWV: Square wave voltammetry

The selectivity and interference effect on the electrochemical response of Au NPs@c-MWCNTs/GCE to determination of 100 μg/l dicapthon were studied at scan rate of 10mV/s in 0.1M PBS (pH7.0). Nitrophenol components such as 2-nitrophenol, 3-nitrophenol, 4-nitrophenol may interfere with the simultaneous detection of dicapthon. 500 μg/l of this component had been investigated with the Au NPs@c-MWCNTs/GCE. In addition, the electrode responses in presence of 500 μg/l of Pb^{2+}, Cd^{2+}, Co^{2+}, Cu^{2+} and Mg^{2+} were also recorded.

Table 2. The recorded electrocatalytic currents of DPV responses to dicapthon and various substances on Au NPs@c-MWCNTs/GCE under applied potential from -0.4 to 0.5V at scan rate of 10mV/s in 0.1M PBS (pH 7.0).

Interfering substance	**Added (μg/l)**	**Electrocatalytic current response (μA)**	**RSD (%)**
dicapthon	100	0.323	±0.003
2-nitrophenol	500	0.017	±0.004
3-nitrophenol	500	0.018	±0.003
4-nitrophenol	500	0.016	±0.002
Pb^{2+}	500	0.011	±0.001
Cd^{2+}	500	0.012	±0.004
Co^{2+}	500	0.010	±0.002
Cu^{2+}	500	0.011	±0.003
Mg^{2+}	500	0.013	±0.004

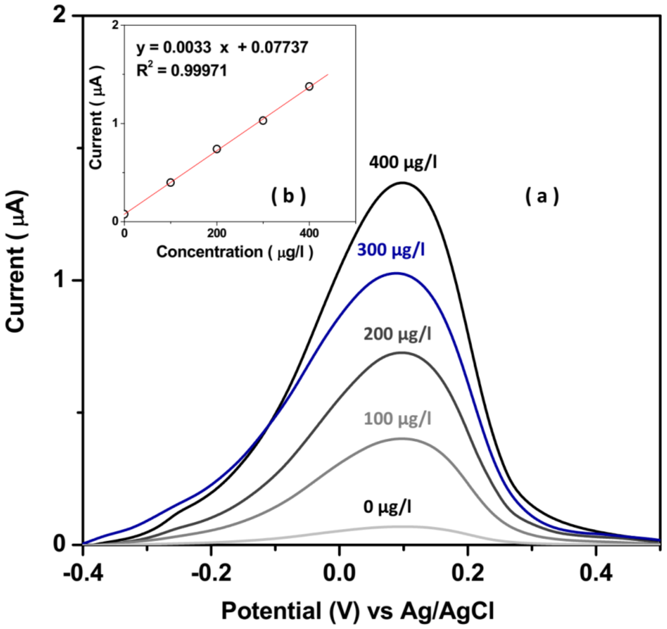

Figure 8. (a) The recorded DPVs and (b) calibration plot of Au NPs@c-MWCNTs/GCE to successive additions of 100 μg/l dicapthon solutions (0 to 400μg/l) under applied potential from -0.4 to 0.5V at scan rate of 10mV/s in 0.1M PBS (pH7.0) including real samples.

The recorded response currents for the addition of dicapthon at the Au NPs@c-MWCNTs/GCE are compared with the recorded response in the presence of a 5-fold higher content of interfering substances in Table 2 which indicated none caused any remarkable interference on the dicapthon sensor performance.

To evaluate the feasibility of Au NPs@c-MWCNTs/GCE for dicapthon detection, the dicapthon sprayed cabbage selected as a real sample. Figure 8a shows the recorded DPV responses to successive additions of 100 µg/l dicapthon solutions under applied potential from -0.4 to 0.5V at scan rate of 10mV/s in 0.1M PBS (pH7.0). As observed from Figure 8a, well-defined DPV responses are obtained for each injection of dicapthon in the electrochemical cell containing real samples. The calibration plot in Figure 8b shows good linearity and the dicapthon content in electrochemical cells and real samples are obtained 23.44 and 46.89 µg/l, respectively. Thus, the dicapthon concentration in initial cabbage (without spraying 40 µg/l of dicapthon solution) is obtained 6.89 µg/l. The analytical applicability of the Au NPs@c-MWCNTs/GCE was studied to determine dichlorvos in a prepared real sample by standard addition method. Table 3 illustrates acceptable values for recovery (94.16% to 97.40%) and RSD (2.51%-4.63%) that it implied the proposed sensor has reliable performance for the determination of dicapthon in agricultural food.

Table 3. Analytical results of Au NPs@c-MWCNTs/GCEto determination dicapthon in real samples.

Sample	Added (µg/l)	Found (µg/l)	Recovery (%)	RSD (%)
cabbage	100.0	97.4	97.40	3.17
	200.0	189.0	94.50	2.51
	300.0	291.5	97.16	4.17
	400.0	387.7	96.92	4.63

4. CONCLUSION

This study focused on the preparation and characterization of electrochemical sensors based on Au NPs@c-MWCNTs nanocomposite for determination of dicapthon pesticide in agricultural food. Au NPs@c-MWCNTs nanocomposite was electrodeposited on GCE. The surface morphologies and crystal structure of the modified electrode were characterized via SEM and XRD analyses, which indicated the spherical Au NPs in fcc crystal structure were uniformly distributed in entangled texture of c-MWCNTs. The electrochemical studies of GCE, MWCNTs/GCE and Au NPs@c-MWCNTs/GCE showed that the Au NPs@c-MWCNTs/GCE exhibited more stable, sharp and higher reduction peak current in presence of dicapthon which related to the electron transfer enhancement between analyte and electrode surface due to interface efficiently of MWCNTs and Au NPs. Moreover, the linear range and detection limit were obtained 0 to 2400 µg/l and 0.09 µg/l, respectively. The selectivity and interference effect on the electrochemical response of Au NPs@c-MWCNTs/GCE for determination of dicapthon were studied. The feasibility of the papered electrode was evaluated for dicapthon detection in cabbage as a real sample.

References

1. M.B. Colovic, D.Z. Krstic, T.D. Lazarevic-Pasti, A.M. Bondzic and V.M. Vasic, *Current neuropharmacology*, 11(2013)315.
2. H. Karimi-Maleh, M. Alizadeh, Y. Orooji, F. Karimi, M. Baghayeri, J. Rouhi, S. Tajik, H. Beitollahi, S. Agarwal and V.K. Gupta, *Industrial & Engineering Chemistry Research*, 60(2021)816.
3. H. Zhang, X. Yuan, T. Xiong, H. Wang and L. Jiang, *Chemical Engineering Journal*, 15(2020)125657.
4. L. Rani, K. Thapa, N. Kanojia, N. Sharma, S. Singh, A.S. Grewal, A.L. Srivastav and J. Kaushal, *Journal of Cleaner Production*, 41(2020)124657.
5. J. Rouhi, S. Kakooei, S.M. Sadeghzadeh, O. Rouhi and R. Karimzadeh, *Journal of Solid State Electrochemistry*, 24(2020)1599.
6. G. Georgiadis, C. Mavridis, C. Belantis, I. Zisis, I. Skamagkas, I. Fragkiadoulaki, I. Heretis, V. Tzortzis, K. Psathakis and A. Tsatsakis, *Toxicology*, 406(2018)129.
7. L. Chedik, A. Bruyere and O. Fardel, *Xenobiotica*, 49(2019)363.
8. R. Liman, *Cytotechnology*, 66(2014)741.
9. H. Karimi-Maleh, S. Ranjbari, B. Tanhaei, A. Ayati, Y. Orooji, M. Alizadeh, F. Karimi, S. Salmanpour, J. Rouhi and M. Sillanpää, *Environmental Research*, 195(2021)110809.
10. J.R. Voorhees, D.S. Rohlman, P.J. Lein and A.A. Pieper, *Frontiers in neuroscience*, 10(2017)590.
11. J. Rouhi, S. Kakooei, M.C. Ismail, R. Karimzadeh and M.R. Mahmood, *International Journal of Electrochemical Science*, 12(2017)9933.
12. B. Albero, C. Sánchez-Brunete and J.L. Tadeo, *Journal of agricultural and food chemistry*, 51(2003)
13. T. Jeyapragasam, R. Saraswathi, S.-M. Chen and T.-W. Chen, *International Journal of Electrochemical Science*, 12(2017)4768.
14. T. Jeyapragasam, R. Saraswathi, S.-M. Chen and B.-S. Lou, *International Journal of Electrochemical Science*, 8(2013)12353.
15. J. Jiang, H. Zhang, C. Wang and Y. Xu, *International Journal of Electrochemical Science*, 11(2016)5481.
16. C. Wang, Q. Song, X. Liu and X. Zhu, *International Journal of Electrochemical Science*, 15(2020)5623.
17. N. Xia and Y. Gao, *International Journal of Electrochemical Science*, 10(2015)713.
18. H. Karimi-Maleh, Y. Orooji, A. Ayati, S. Qanbari, B. Tanhaei, F. Karimi, M. Alizadeh, J. Rouhi, L. Fu and M. Sillanpää, *Journal of Molecular Liquids*, 329(2021)115062.
19. S. Changaei, J. Zamir-Anvari, N.-S. Heydari, S.G. Zamharir, M. Arshadi, B. Bahrami, J. Rouhi and R. Karimzadeh, *Journal of Electronic Materials*, 48(2019)6216.
20. H. Savaloni, R. Savari and S. Abbasi, *Current Applied Physics*, 18(2018)869.
21. R. Savari, H. Savaloni, S. Abbasi and F. Placido, *Sensors and Actuators B: Chemical*, 266(2018)620.
22. F. Olorundare, D. Nkosi and O. Arotiba, *International Journal of Electrochemical Science*, 11(2016)7318.
23. F. Chahshouri, H. Savaloni, E. Khani and R. Savari, *Journal of Micromechanics and Microengineering*, 30(2020)075001.
24. J. Rouhi, S. Mahmud, S.D. Hutagalung, N. Naderi, S. Kakooei and M.J. Abdullah, *Semiconductor Science and Technology*, 27(2012)065001.
25. J. Wang, *Microchimica Acta*, 177(2012)245.
26. I.-H. Cho, D.H. Kim and S. Park, *Biomaterials research*, 24(2020)1.

27. D. Thomas, Z. Rasheed, J.S. Jagan and K.G. Kumar, *Journal of food science and technology*, 52(2015)6719.
28. Z. Savari, S. Soltanian, A. Noorbakhsh, A. Salimi, M. Najafi and P. Servati, *Sensors and Actuators B: Chemical*, 176(2013)335.
29. A.J. MacLeod, *Applied mathematics and computation*, 57(1993)305.
30. G. Liu and Y. Lin, *Analytical chemistry*, 77(2005)
31. P. Prasad and N. Sreedhar, *Chemical Methodologies*, 2(2018)277.
32. T. Wirtanen, E. Rodrigo and S.R. Waldvogel, *Advanced Synthesis & Catalysis*, 362(2020)2088.
33. B. Wu, Z. Ou, X. Ju and S. Hou, *Journal of Nanomaterials*, 2011(2011)464919.
34. K. Lata, V. Dhull and V. Hooda, *Biochemistry Research International*, 2016(2016)1545206.
35. K. Manojkumar, A. Sivaramakrishna and K. Vijayakrishna, *Journal of Nanoparticle Research*, 18(2016)103.
36. C. Li, C. Wang, Y. Ma, W. Bao and S. Hu, *Analytical and Bioanalytical Chemistry*, 381(2005)1049.
37. J. Mehta, N. Bhardwaj, S.K. Bhardwaj, S.K. Tuteja, P. Vinayak, A.K. Paul, K.-H. Kim and A. Deep, *Analytical Biochemistry*, 523(2017)1.
38. A. Deep, S.K. Bhardwaj, A. Paul, K.-H. Kim and P. Kumar, *Biosensors and bioelectronics*, 65(2015)226.
39. M. Guler, V. Turkoglu and A. Kivrak, *Environmental Science and Pollution Research*, 23(2016)12343.
40. D. Huo, Q. Li, Y. Zhang, C. Hou and Y. Lei, *Sensors and Actuators B: Chemical*, 199(2014)410.
41. X. Yan, H. Li, X. Wang and X. Su, *Talanta*, 131(2015)88.
42. M. Govindasamy, S.-M. Chen, V. Mani, M. Akilarasan, S. Kogularasu and B. Subramani, *Microchimica Acta*, 184(2017)725.
43. M. Musameh, M.R. Notivoli, M. Hickey, C.P. Huynh, S.C. Hawkins, J.M. Yousef and I.L. Kyratzis, *Electrochimica Acta*, 101(2013)209.
44. F. Arduini, M. Forchielli, A. Amine, D. Neagu, I. Cacciotti, F. Nanni, D. Moscone and G. Palleschi, *Microchimica Acta*, 182(2015)643.